

Determining the Permittivity of NaCl & CH₃OH via an Equivalent Circuit Model

Abstract

In this project, our objective is to develop a radiating antenna model accurately simulating the behavior of a coaxial transmission line, following Marsland and Evans' methodology. The study involves deriving the antenna model based on their method and comparing it with a conventional equivalent circuit approach to determine the complex permittivities of methanol (CH₃OH) and sodium chloride (NaCl). The obtained complex permittivities exhibited remarkable consistency with theoretical predictions at high frequencies but demonstrated less accuracy at lower frequencies. This discrepancy indicates that while the proposed antenna model effectively represents the behavior of the coaxial transmission line, its accuracy diminishes at lower frequencies. Nonetheless, the close agreement between experimental and theoretical values at high frequencies confirms the model's robustness, affirming its suitability for practical applications in antenna design and optimization.

1 INTRODUCTION & THEORETICAL BACKGROUND

James Clerk Maxwell is well-known for his pioneering work in electromagnetism, which is fundamental to modern physics and industry. Maxwell presented his breakthrough theory of electric and magnetic fields to the Royal Society of London in 1865. This theory gave rise to a thorough framework for comprehending the behaviour of electromagnetic fields, which was condensed into four concise equations that are now known as Maxwell's equations. Despite the original complexity of his concepts, Maxwell's equations became fundamental principles in physics and engineering, paving the way for advances in telecommunications, electrical engineering, and a variety of other disciplines (Rautio, 2014).

When electromagnetic waves encounter boundaries between different materials, such as air and glass or air and metal, an interesting interaction takes place. A portion of the wave reflects back, while the rest penetrates into the new medium. This reflection phenomenon is quantified by the reflection coefficient, a complex number that describes the ratio of reflected wave magnitude to incident wave magnitude. Its real part signifies the magnitude of reflection relative to incidence wave, while the imaginary part denotes phase shift. (Šarolić & Matković, 2022).

In order to understand how electromagnetic waves interact with materials, one must investigate on a property called complex permittivity, ϵ . This property expands on permittivity, accounting for electrical conductivity and dielectric losses within materials. Complex permittivity, is represented as a complex number, which consists of a real part, ϵ' and imaginary part, ϵ'' .

The real part of complex permittivity measures a material's ability to store electrical energy when exposed to an electric field (Šarolić & Matković, 2022). It denotes the material's ability to polarise in response to an external electric field. When an electric field is applied, the charges in the material shift causing polarisation. A higher real part of permittivity indicates a stronger polarisation response and, as a result, a greater ability of the

material to store energy. Materials with high dielectric constants are often used in capacitors and other energy storage devices.

The imaginary part of complex permittivity represents energy dissipation or loss within the material when exposed to an electric field. It describes numerous ways by which the material absorbs and dissipates energy from the electric field. Materials with higher imaginary parts suffer more losses when interacting with electromagnetic waves. These losses show as heating or attenuation of the wave as it travels through the material (Von Hippel & Labounsky, 1995). Understanding the imaginary part is critical in applications requiring little energy loss, such as telecommunications systems. The ratio of the permittivity's imaginary to real parts is quantified by the tangent delta function. It is used to quantify how much a material loses or dissipates in the presence of an alternating electric field. Greater energy loss tendency is indicated by higher tangent delta values, which also imply a more evident dissipative behavior in the material's dielectric response.

$$\tan \delta = \frac{\epsilon''}{\epsilon'} \quad (\check{S}arolić & Matković, 2022) \quad (1)$$

Where the complex permittivity ϵ^* is defined as,

$$\epsilon = \epsilon' - i\epsilon'' \quad (\text{Von Hippel & Labounsky, 1995}) \quad (2)$$

Theoretical basis in modelling coaxial transmission lines as radiating antennas is critical for understanding their behaviour and applications in a variety of sectors. Coaxial cables, which consist of inner and outer conductors separated by a dielectric substance, are widely used for signal transmission due to their capacity to restrict electromagnetic fields within the cable (Marcuvitz, 1951). The transverse electromagnetic (TEM) mode is the primary mode of propagation in coaxial cables, in which both electric and magnetic fields are transverse to the propagation direction (Marsland & Evans, 1987). When a coaxial cable is terminated with an open circuit, it becomes a radiating antenna, sending electromagnetic waves into the surrounding medium in the given document.

Deschamps' insight plays a crucial role in coaxial antenna modeling by establishing a connection between the antenna's admittance and the dielectric properties of the surrounding medium (Deschamps, 1962). To capture the intricate interactions between the antenna and its environment, equivalent circuit models are developed. These models account for the geometry of the open-ended coaxial construction and the distribution of electromagnetic fields. They typically incorporate lumped elements such as resistors, capacitors, and inductors to represent the dispersed properties of the coaxial cable and radiation effects at the open end (Brandy et al., 1981). Additionally, the presence of fringing fields beyond the coaxial limits influences the antenna's radiation pattern and impedance characteristics. These models can then be leveraged to derive an expression for the complex permittivity of an unknown material.

Another approach is based on rigorous electromagnetic simulations, such as finite element analysis (FEA) or finite difference time domain (FDTD) simulations. These numerical techniques solve Maxwell's equations in

the time or frequency domain, allowing for the accurate modeling of electromagnetic fields and their interactions with the coaxial structure and surrounding medium (Analysis, n.d.). These simulations can provide insight into the distribution of electromagnetic fields and make it possible to calculate the complicated permittivity of the medium by integrating suitable boundary conditions and material parameters (Chen, 2004).

The aim of this project is to achieve two primary objectives: first, to derive a radiating antenna model approximating a coaxial transmission line using the methodology proposed by Marsland and Evans. Second, to determine the complex permittivity values of sodium chloride (NaCl) and methanol (CH_3OH) at different frequencies. Additionally, we will verify that the obtained complex permittivity values for NaCl and methanol closely match experimental data, thereby confirming the accuracy of the radiating antenna model.

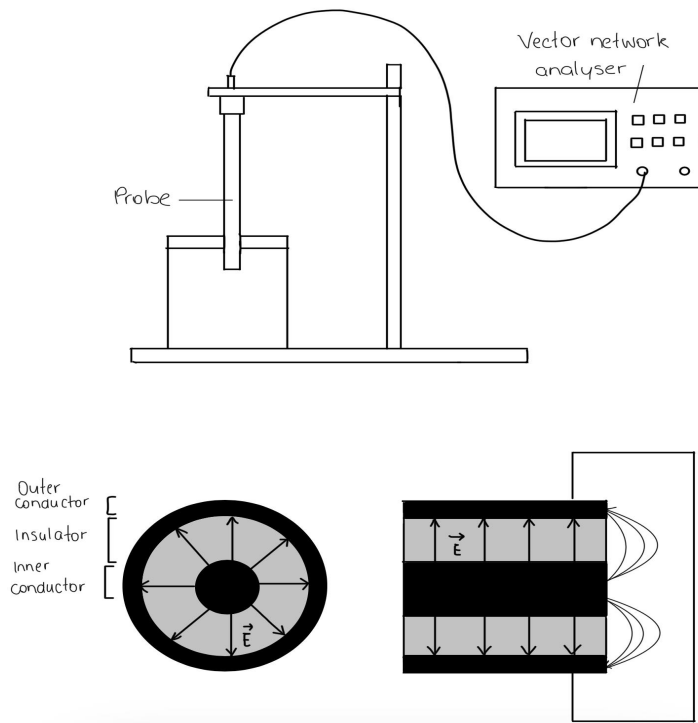


Fig. 1. Showing the setup of the coaxial probe technique for determination of the permittivity (La Gioia et al., 2018)

2 MATERIALS & COMPUTATIONAL TOOLS

The primary code was developed in Python, with pandas and matplotlib libraries utilized for efficient data handling and visualization. Pandas facilitated data organization through data frames (excel), while Matplotlib enabled the creation of various plots showing the permittivity of NaCl and methanol against frequency. The depiction of the experimental setup with the coaxial line is shown in figure 1, while its corresponding equivalent circuit is displayed in figure 2.

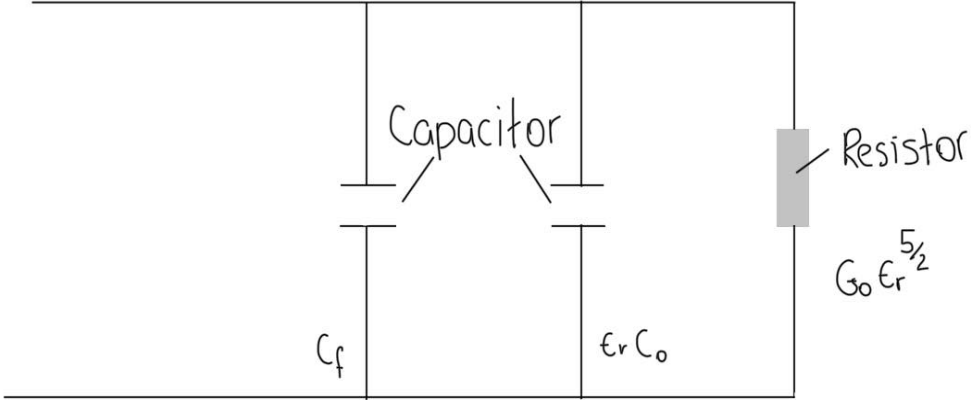


Fig. 2. Showing the Equivalent circuit corresponding to figure 1. G_0 is the free space radiation conductance, C_0 is the capacitance representing the fringing field in external dielectric material while C_f represent the capacitance of the fringing field in the Teflon dielectric (of the cable) (Marsland & Evans, 1987).

3 METHODOLOGY

Starting from the Deschamps modelling theorem,

$$Y(\omega, \epsilon_r \epsilon_0) = \sqrt{\epsilon_r} Y(\omega \sqrt{\epsilon_r}, \epsilon_0) \quad (3)$$

where Y, ϵ_r are the antenna admittance and complex permittivity of the material being under test (where the antenna is embedded), ω is the angular frequency and ϵ_0 is the permittivity of free space.

Note that the admittance is given by,

$$Z = \frac{1}{Y} = Z_0 \frac{1 - \Gamma}{1 + \Gamma} \quad (4)$$

where Z is the impedance, Z_0 is the characteristic impedance and Γ is the reflection coefficient.

Now equation 3 applies if the radiation field by the probe is fully contained within the medium. However an expression for the admittance of the equivalent circuit for the coaxial aperture radiating into free space, where the dimensions are relatively small compared to the wavelength (at some frequencies) is given by,

$$Y(\omega, \epsilon_0) = A\omega^4 + jB\omega \quad (5)$$

where A and B are functions of spatial geometry only.

Now applying equation 3 to equation 5 to get,

$$Y(\omega, \epsilon_r \epsilon_0) = G_0(\omega) \epsilon_r^{5/2} + j\omega C_0 \epsilon_r \quad (6)$$

The fringing field is represented by the capacitance C_0 and the free space radiation conductance $G_0(w)$. $G_0(w)$ indicates how well the antenna converts electric signals into electromagnetic waves that propagate in free space. However, equation 6 is not entirely valid. Since, Equation 3 cannot be applied because the field at the tip of the probe was assumed to be fully transverse electromagnetic mode (TEM), which is not the case. Additionally, equation 5 was derived for the coaxial aperture in an infinite ground plane, which is also not true (Marsland & Evans, 1987)

Brady et al. proposed a solution to address such challenges by suggesting that the equivalent circuit capacitance could be divided into two distinct terms. They proposed that one capacitance, denoted as C_f , represents the fringing field within the transmission line. and additionally, they introduced another parallel capacitance, $\varepsilon_r C_0$, to account for the fringing field outside the transmission line (Brady et al., 1981). Typically, the value of C_0 exceeds that of C_f . This is illustrated in figure 2. Therefore,

$$Y(\omega, \varepsilon_r) = G_0(\omega) \varepsilon_r^{5/2} + j\omega Z_0(\varepsilon_r C_0) + j\omega Z_0(C_f) \quad (7)$$

which can be simplified to,

$$Y(\omega, \varepsilon_r) = G_0(\omega) \varepsilon_r^{5/2} + j\omega Z_0(\varepsilon_r C_0 + C_f) \quad (\text{Admittance model I}) \quad (8)$$

For coaxial lines with dimensions relatively small with the wavelength, we can neglect G_0 since, $G_0 \ll \omega C_0$. Thus,

$$y(\omega, \varepsilon_r) = j\omega Z_0(\varepsilon_r C_0 + C_f) \quad (\text{Admittance model II}) \quad (9)$$

In order to determine the permittivity of dielectric, the input reflection coefficient (probe) must be measured. As explained in Marsland and Evans paper one can use a network-analyser system to measure such coefficient. This is given by :

$$\Gamma_m = \frac{\rho_m - S_{11}}{\rho_m S_{22} - (S_{11} S_{22} - S_{12} S_{21})} \quad (10)$$

where Γ_m is the true reflection coefficient, ρ_m the measured reflection coefficient and $S_{11}, S_{22}, S_{12}, S_{21}$ are the scattering error parameters of the network from the error matrix \mathbf{S} .

Moreover the scattering error parameters of the network are given by:

$$S_{11} = \frac{\Gamma_1 \Gamma_2 \rho_3 (\rho_1 - \rho_2) + \Gamma_1 \Gamma_3 \rho_2 (\rho_3 - \rho_1) + \Gamma_2 \Gamma_3 \rho_1 (\rho_2 - \rho_3)}{\Gamma_1 \Gamma_2 (\rho_1 - \rho_2) + \Gamma_1 \Gamma_3 (\rho_3 - \rho_1) + \Gamma_2 \Gamma_3 (\rho_2 - \rho_3)} \quad (11)$$

$$S_{22} = \frac{\Gamma_1 (\rho_2 - S_{11}) + \Gamma_2 (S_{11} - \rho_1)}{\Gamma_1 \Gamma_2 (\rho_2 - \rho_1)} \quad (12)$$

$$S_{12}S_{21} = \frac{(\rho_1 - S_{11}) - (1 - S_{22}\Gamma_1)}{\Gamma_1} \quad (13)$$

Where $\Gamma_1, \Gamma_2, \Gamma_3$ are the reflective coefficient of terminations used for calibration and ρ_1, ρ_2, ρ_3 are their measured reflective coefficients (Kraszewski et al., 1983).

Substituting equations 11, 12, 13 in equation 10 and rearranging for the admittance y_m correspond to the reflective coefficient ρ_m ,

$$y_m = -\frac{\Delta_{m1}\Delta_{32} y_3 y_2 + \Delta_{m2}\Delta_{13} y_1 y_3 + \Delta_{m3}\Delta_{21} y_2 y_1}{\Delta_{m1}\Delta_{32} y_1 + \Delta_{m2}\Delta_{13} y_2 + \Delta_{m3}\Delta_{21} y_3} \quad (14)$$

where $\Delta_{ij} = \rho_i - \rho_j$

equation 14 follows from the cross-ratio transform, since there is a bilinear relationship between Γ_i and y_i and Γ_i and ρ_i . That is,

$$\frac{\Delta_{m1}\Delta_{32}}{\Delta_{m2}\Delta_{13}} = \frac{(\rho_m - \rho_1)(\rho_3 - \rho_2)}{(\rho_m - \rho_2)(\rho_1 - \rho_3)} = \frac{(y_m - y_1)(y_3 - y_2)}{(y_m - y_2)(y_1 - y_3)} \quad (15)$$

3.1 Admittance model I

By applying this cross-ratio invariance property to the probe, it follows that the admittance of the probe is capable of undergoing bilinear transformation. Applying the linear transformation,

$$y'(\omega, \varepsilon_r) = \left(\frac{1}{j\omega C_0 Z_0} \right) y(\omega, \varepsilon_r) - \left(\frac{C_f}{C_0} \right) \quad (16)$$

to equation 8 to get,

$$y'(\omega, \varepsilon_r) = \varepsilon_r + \frac{G_0 \varepsilon_r^{5/2}}{j\omega C_0} \quad (17)$$

simplifying,

$$y'(\omega, \varepsilon_r) = \varepsilon_r + G_n \varepsilon_r^{5/2} \quad (18)$$

where $G_n = \frac{G_0}{j\omega C_0}$ referred to as the normalised radiation conductance

Due to the property of cross-ratio invariance, the admittance, when subjected to linear transformation, still satisfies,

$$\frac{(\rho_m - \rho_1)(\rho_3 - \rho_2)}{(\rho_m - \rho_2)(\rho_1 - \rho_3)} = \frac{(y'_m - y'_1)(y'_3 - y'_2)}{(y'_m - y'_2)(y'_1 - y'_3)} \quad (19)$$

if we cross multiply, we can set y'_m subject of the formula and equate it to equation 18 to obtain,

$$0 = \varepsilon_m + G_n \varepsilon_m^{5/2} + \left[\frac{\Delta_{m1}\Delta_{32} y'_3 y'_2 + \Delta_{m2}\Delta_{13} y'_1 y'_3 + \Delta_{m3}\Delta_{21} y'_2 y'_1}{\Delta_{m1}\Delta_{32} y'_1 + \Delta_{m2}\Delta_{13} y'_2 + \Delta_{m3}\Delta_{21} y'_3} \right] \quad (20)$$

It follows that the coefficients of the polynomial are functions of the permittivities and their respective reflection coefficient, $(\varepsilon_1, \varepsilon_2, \varepsilon_3)$ and (ρ_1, ρ_2, ρ_3) .

What remains is solving for G_n , this can be accomplished by introducing a known dielectric with known permittivity and reflection coefficient. Once G_n is determined, it can be used to determine the permittivity of various unknown materials through numerical solutions.

3.2 Short Circuit Simplification

If we use a short circuit, we know by definition that the admittance goes to infinity, since the impedance approaches zero. Since,

$$Y = \frac{1}{Z} \quad (21)$$

and

$$\lim_{Z \rightarrow 0} Y = \infty. \quad (22)$$

Note that for our experiment ρ_1 correspond to the short-circuit reflective coefficient, ρ_2 corresponds air reflective coefficient and ρ_3 corresponds to distilled water reflective coefficient. Correspondingly, their respective permittivities are denoted by $\varepsilon_1, \varepsilon_2, \varepsilon_3$.

thus as $y_1 \rightarrow \infty$ equation 20 becomes,

$$\varepsilon_m + G_n \varepsilon_m^{5/2} + \left[\frac{\Delta_{m2}\Delta_{13} y'_3 + \Delta_{m3}\Delta_{21} y'_2}{\Delta_{m1}\Delta_{32}} \right] = 0 \quad (23)$$

Again one can in turn determine G_n by again introducing a new material with known permittivity ε_4 and reflection coefficient ρ_4 and setting $m = 4$.

3.3 Admittance model II

Since G_n is generally small we can neglect, and approximate the permittivity ε_m as,

$$\varepsilon_m + \left[\frac{\Delta_{m2}\Delta_{13} y'_3 + \Delta_{m3}\Delta_{21} y'_2}{\Delta_{m1}\Delta_{32}} \right] = 0 \quad (24)$$

setting ε_m subject of the formula to get

$$\varepsilon_m = - \left[\frac{\Delta_{m2}\Delta_{13} y'_3 + \Delta_{m3}\Delta_{21} y'_2}{\Delta_{m1}\Delta_{32}} \right] \quad (25)$$

but from equation 18 we know that if G_n is very small, then,

$$y'(\omega, \varepsilon_r) = \varepsilon_r \quad (26)$$

substituting equation 26 in equation 25 to get,

$$\varepsilon_m = -\frac{\Delta_{m2}\Delta_{13}}{\Delta_{m1}\Delta_{32}}\varepsilon_3 - \frac{\Delta_{m3}\Delta_{21}}{\Delta_{m1}\Delta_{32}}\varepsilon_2 \quad (27)$$

thus the permittivity of an unknown material ε_m can be calculated simply by knowing the reflection coefficient ρ_m without any additional information of the equivalent circuit. That is not knowing C_f and C_0 .

4 RESULTS

4.1 Data & plots

Graphs 3, 4, and 5 illustrate the real, imaginary, and absolute values of the complex permittivity of sodium chloride (NaCl) plotted against *frequency* in Hz. The vertical lines indicate the percentage accuracy of the experimental values compared to the theoretical values. Additionally, the residuals, which represent the difference between experimental and theoretical values, are plotted below the main graphs.

Similarly, Graphs 6, 7, and 8 display the real, imaginary, and absolute values of the complex permittivities for methanol (CH₃OH) plotted against *frequency* in Hz. The vertical lines represent the percentage accuracy, and the subplot below illustrates the residuals.

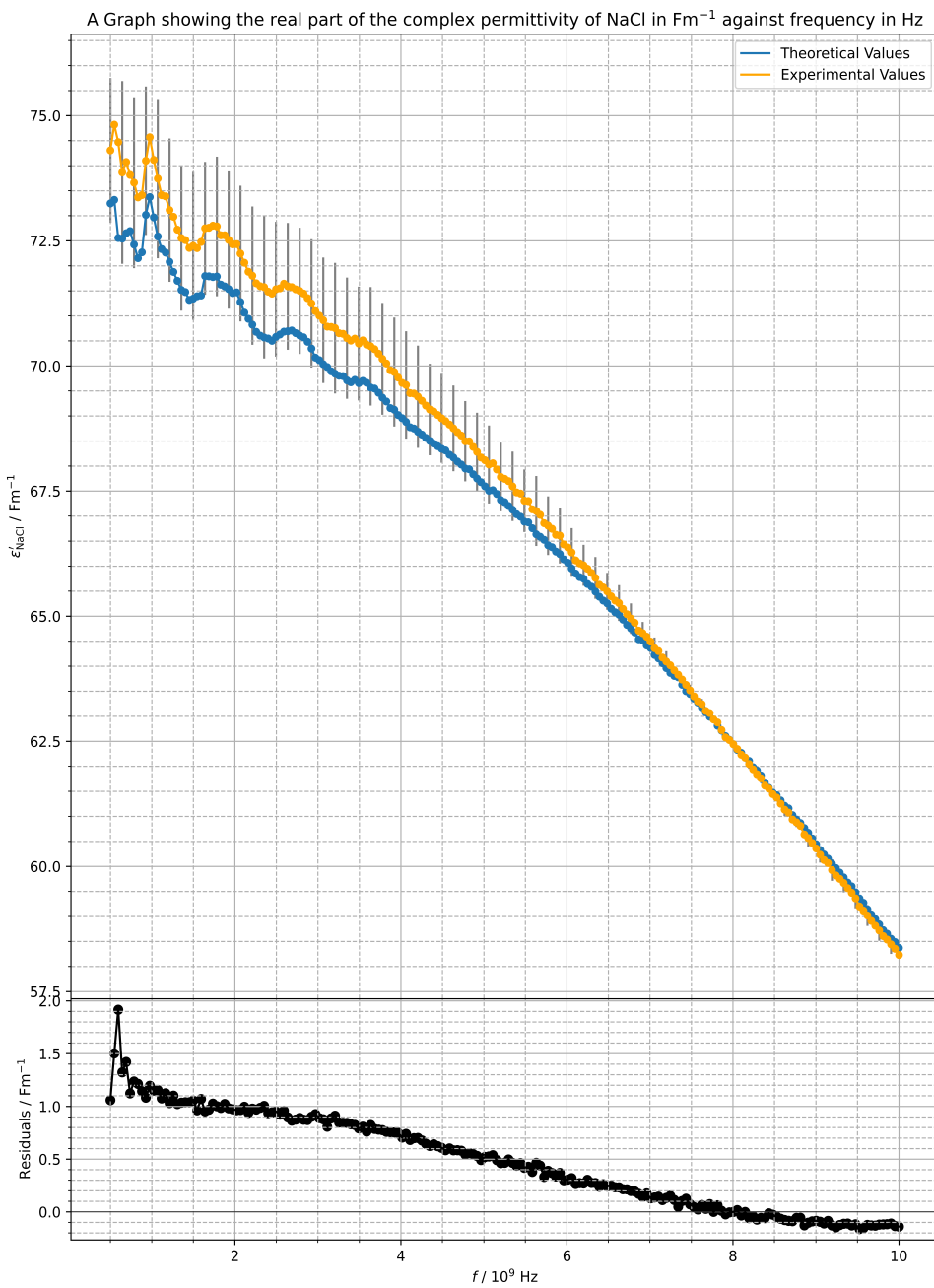


Fig. 3. Showing the real part of the complex permittivity $\varepsilon'_{\text{NaCl}}$ against frequency in Hz for sodium chloride (NaCl).

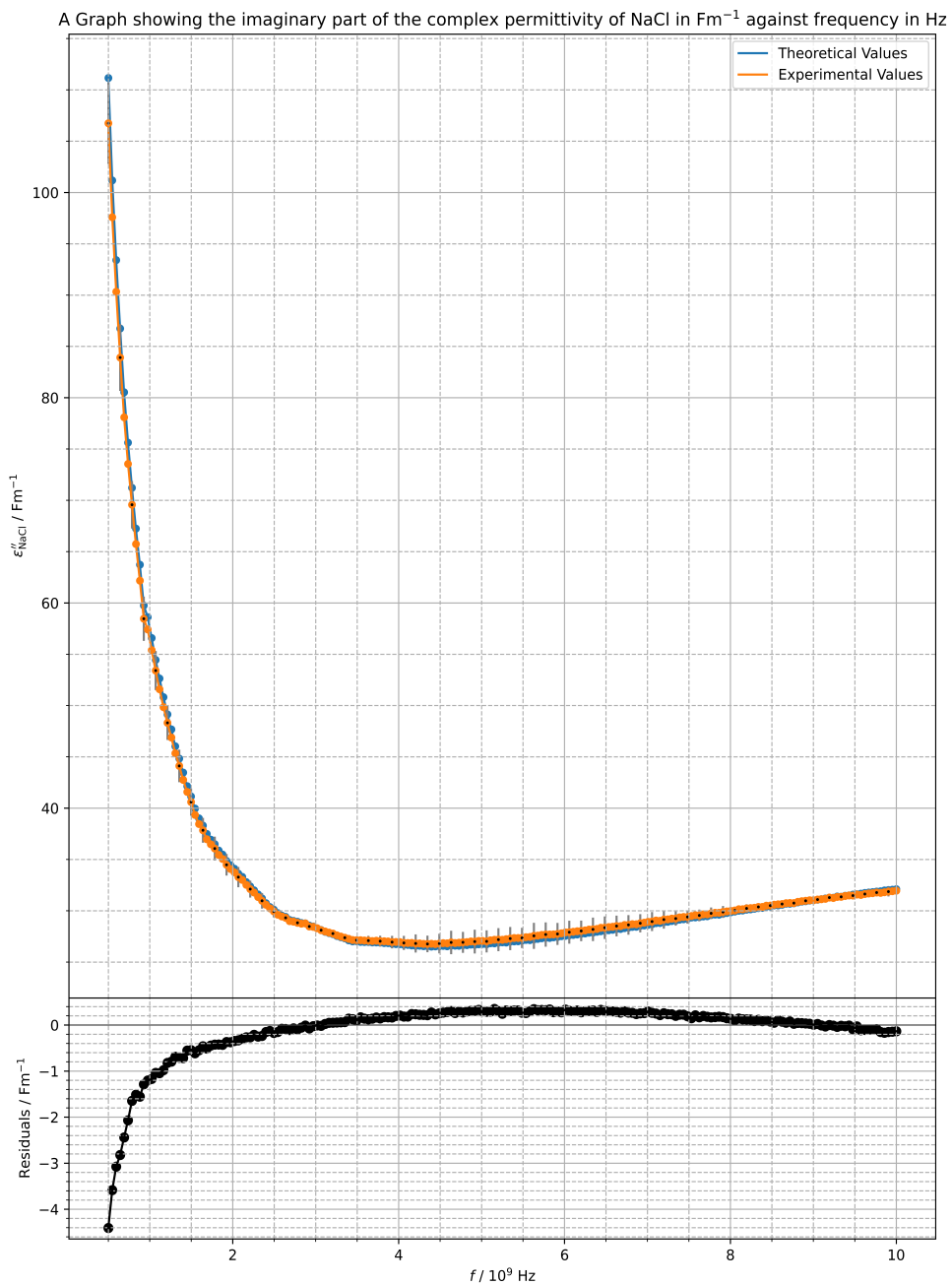


Fig. 4. Showing the imaginary part of the complex permittivity $\varepsilon''_{\text{NaCl}}$ against frequency in Hz for sodium chloride (NaCl).

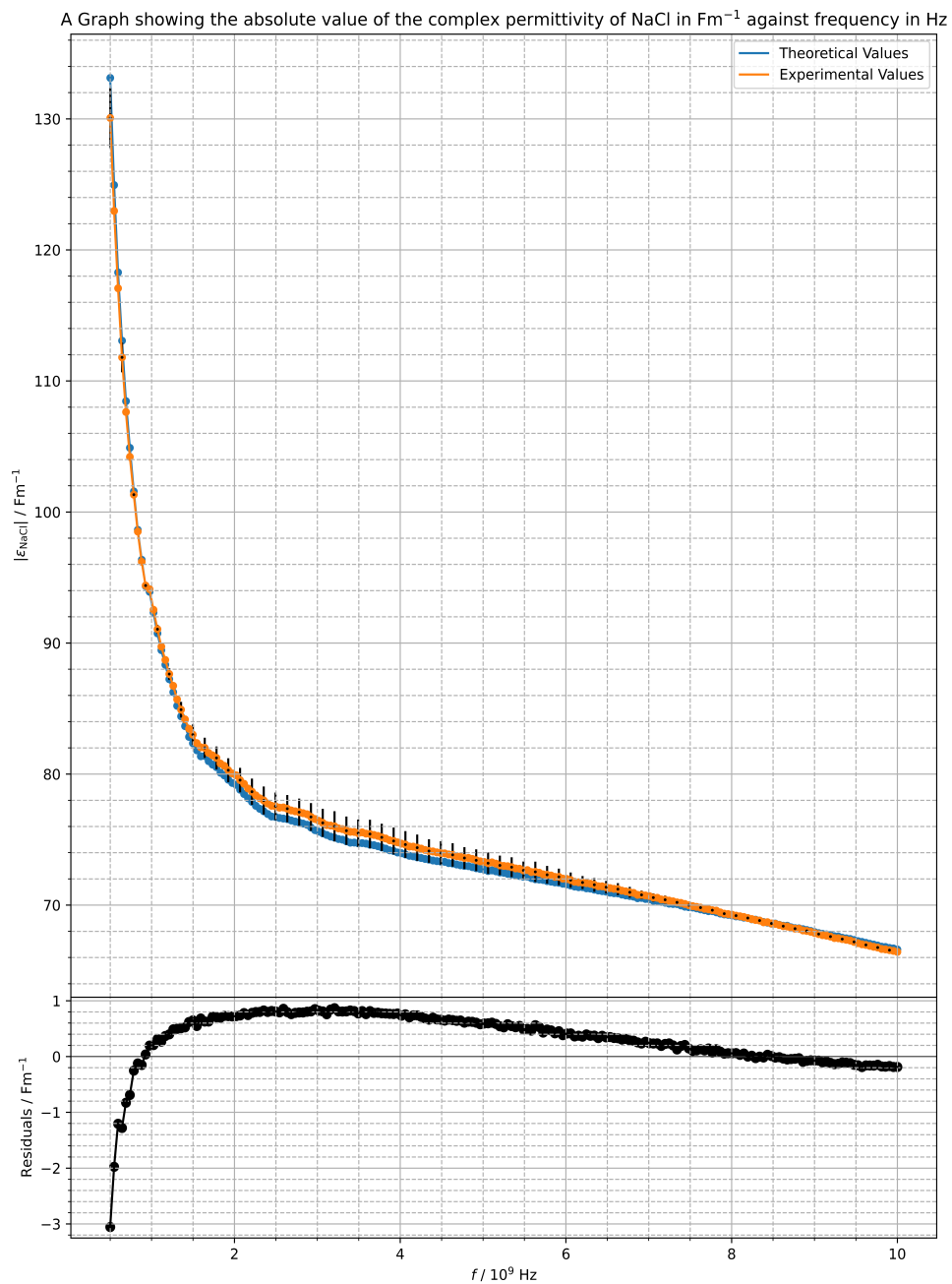


Fig. 5. Showing the absolute value of the complex permittivity $|\epsilon_{\text{NaCl}}|$ against *frequency* in Hz for sodium chloride (NaCl).

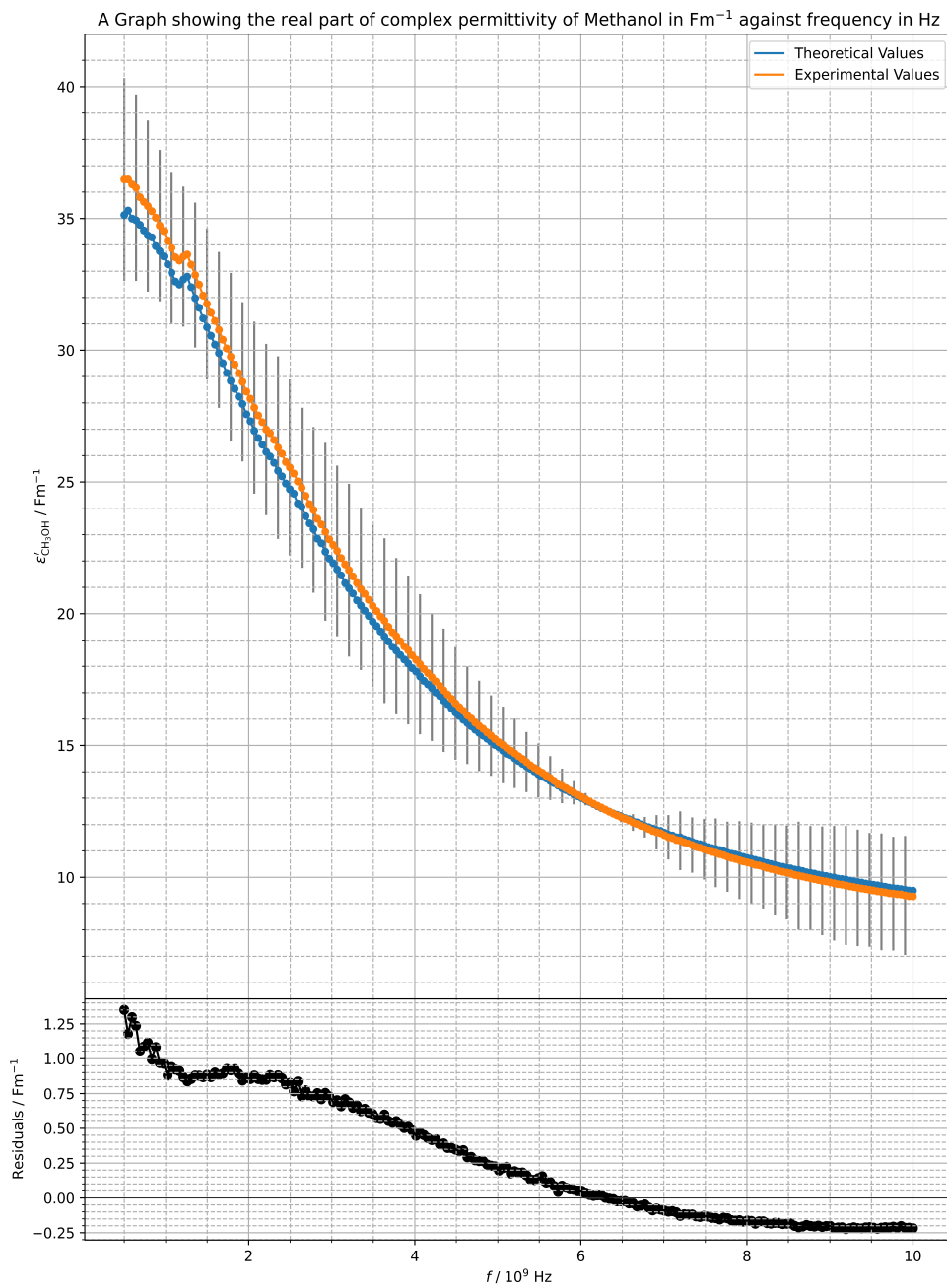


Fig. 6. Showing the real part of the complex permittivity $\epsilon'_{\text{CH}_3\text{OH}}$ against frequency in Hz for methanol (CH_3OH).

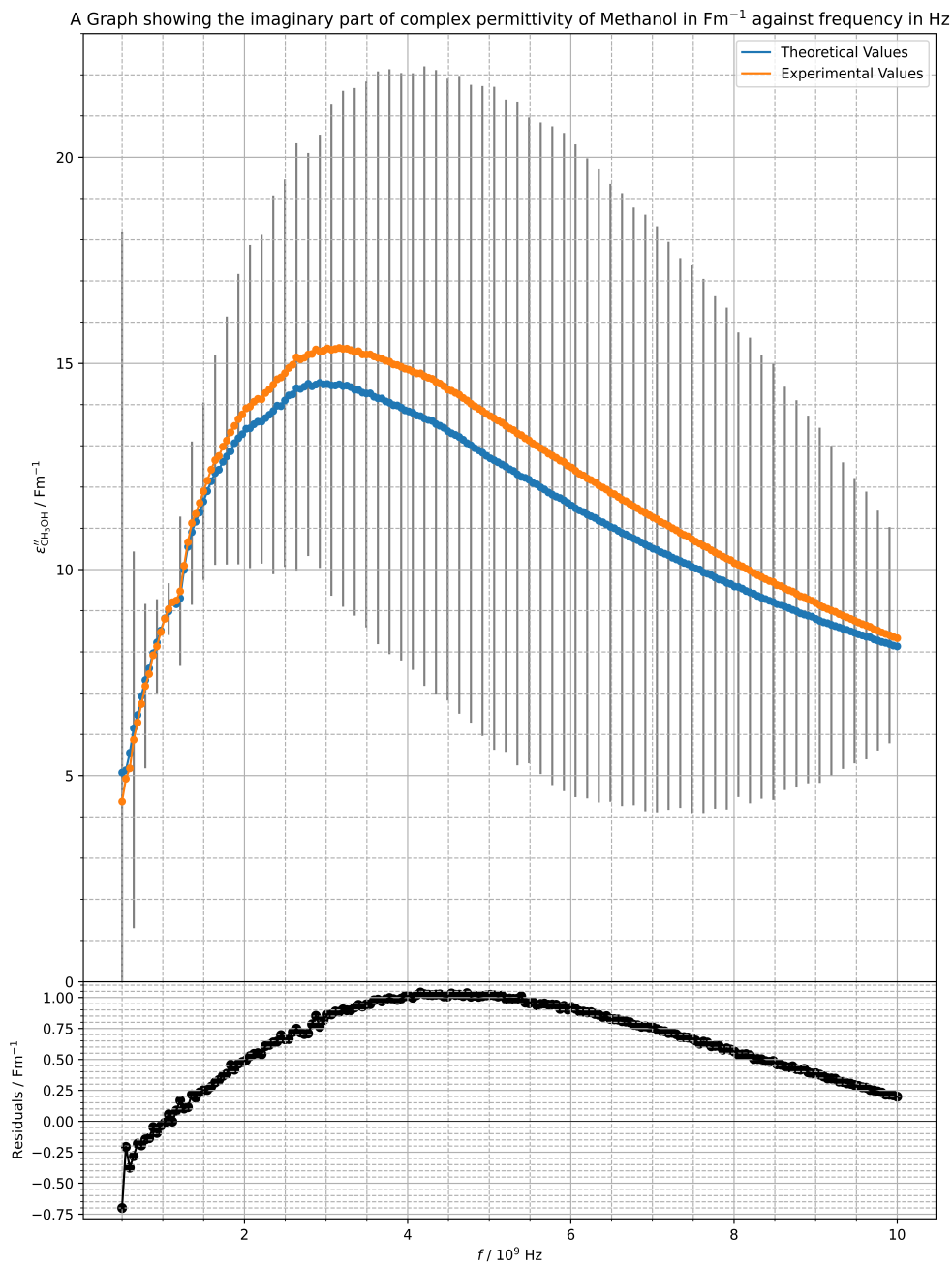


Fig. 7. Showing the imaginary part of the complex permittivity $\epsilon''_{\text{CH}_3\text{OH}}$ against frequency in Hz for methanol (CH_3OH).

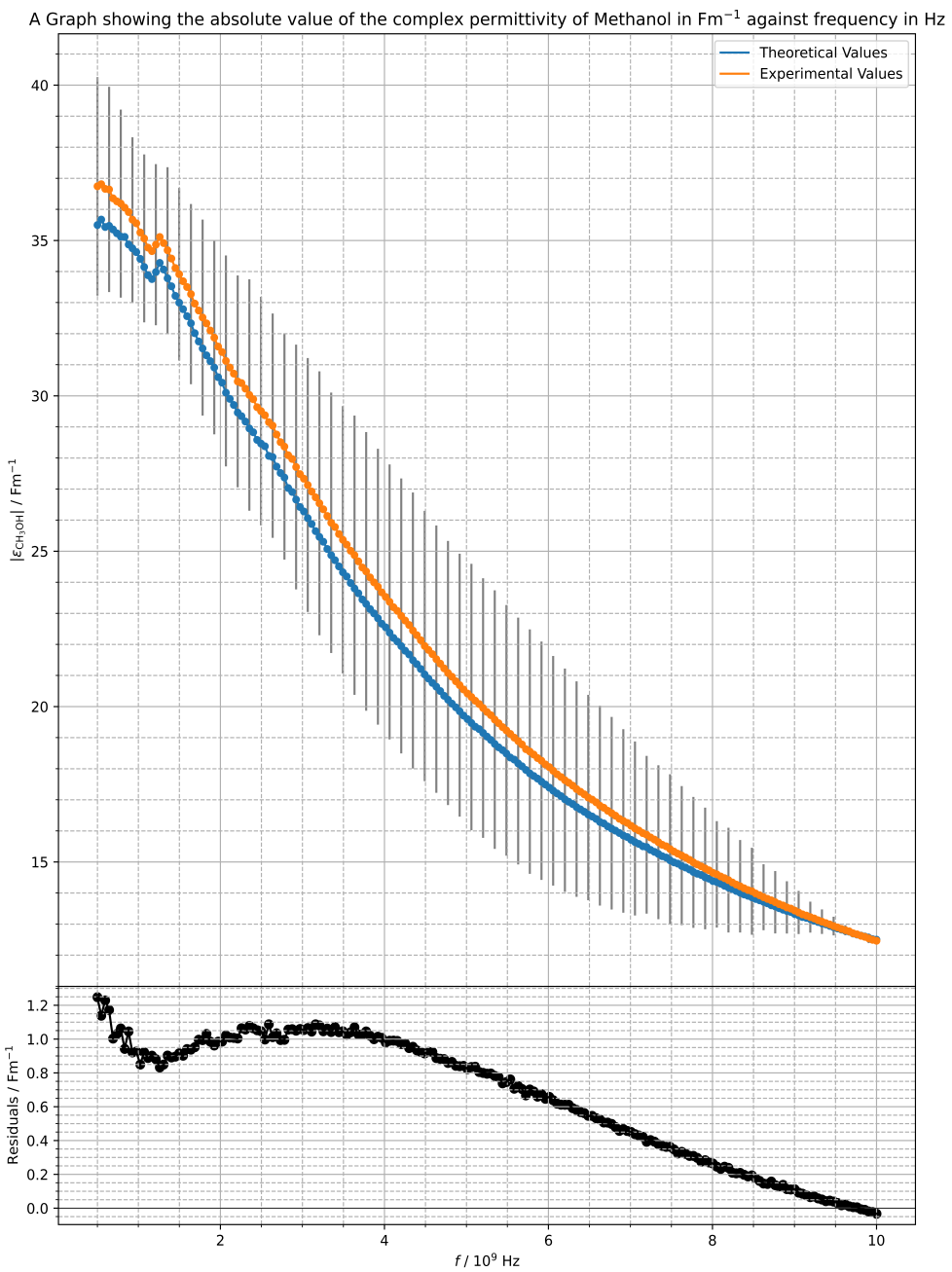


Fig. 8. Showing the absolute value of the complex permittivity $|\epsilon_{\text{CH}_3\text{OH}}|$ against frequency in Hz for methanol (CH_3OH).

5 DISCUSSION

Marsland and Evans' paper offers a method to address systematic errors in network analysis stemming from imperfections inherent in real network-analyzer systems. These imperfections include issues with the test set, cabling, and connectors, which can affect the accuracy of measurements. Conventionally, network-analyzer calibration procedures involve using measurements of known terminations, such as shorts, opens, and matches, that is the reflective coefficient $\Gamma_1, \Gamma_2, \Gamma_3$, to determine the necessary elements of the embedding network's scattering matrix \mathbf{S} as seen in equations 11, 12 and 13. The choice of standard liquid for calibration purposes is crucial to minimizing errors in the calibration process. Specifically, it's important to select a liquid whose permittivity (or dielectric constant) differs substantially from the other known terminations, such as the short circuit Γ_1 and open circuit Γ_2 . This difference helps reduce calibration errors that may arise due to uncertainties in the dielectric properties of the liquid. Generally, liquids meeting this criterion are polar in nature and exhibit significant conductivity. Moreover, their permittivity is frequency-dependent, making it necessary to select liquids whose frequency-dependent permittivity can be described analytically (Kraszewski et al., 1983). Many polar liquids, including water and various alcohols, have permittivity described by equations such as the Debye equation,

$$\epsilon(f) = \epsilon_{\infty} + \frac{\epsilon_s - \epsilon_{\infty}}{1 + (2\pi f \tau)^2} \quad (\text{Kraszewski et al., 1983}) \quad (28)$$

where $\epsilon(f)$ is the permittivity of the material at frequency f . ϵ_{∞} is the permittivity at infinite frequency, which represents the high-frequency limit of the material. ϵ_s is the static permittivity, which represents the permittivity at zero/very low frequency. τ is the relaxation time of the material, which characterizes how quickly the material responds to changes in electric field.

Marsland and Evans propose a different approach that circumvents the need to specify the parameters of the embedding network explicitly. Instead, they suggest substituting known admittance's (y_1, y_2 , and y_3) with corresponding reflection-coefficient measurements (ρ_1, ρ_2 , and ρ_3) into a equation 10, eliminating the terms of the scattering matrix \mathbf{S} between them. This technique simplifies the error correction process by directly deriving an expression for the admittance (y_m) based on existing admittance-reflection coefficient pairings, effectively bypassing the complexities associated with determining the embedding network's parameters (Marsland & Evans, 1987). This streamlined approach offers a more efficient way to obtain an equation for admittance y_m .

For Sodium chloride (NaCl), graph 3 illustrates a lack of accuracy with the theoretical values at low frequencies, as evidenced by the residuals. However, as the frequency increases, it becomes apparent that the experimental and theoretical values converge toward 10 GHz. Similarly, graph 4 displays a comparable trend, showing a lack of accuracy at low frequencies and improved accuracy as the frequency approaches 10 GHz. Graph 5, representing the absolute value of the combination of graphs 3 and 4, follows a similar pattern, exhibiting lower accuracy at low frequencies and higher accuracy towards 10 GHz.

For methanol (CH₃OH), graph 6 demonstrates lower accuracy at low frequencies, with the highest accuracy observed around 6-6.5 GHz, after which it begins to diverge again. Conversely, graph 7 showcases the highest

accuracy at 1 GHz, with accuracy declining beyond this frequency until it starts to converge again towards high accuracy approaching 10 GHz. Similarly, graph 8 follows a trend similar to that of graph 6.

Generally, it can be observed that the experimental values diverge most significantly from the theoretical values at low frequencies. It is important to note that this discrepancy arises from the derivation of Admittance Model II. As explained in the methodology section, G_n is inversely proportional to the frequency f , and during the derivation of Admittance Model II, we omit G_n to simplify the equation. However, at low frequencies, the influence of G_n is most pronounced, whereas as the frequency approaches higher values, a more accurate approximation of the permittivity can be made. It is best summarized by the equation for the permittivity, as shown in Equation 27, which achieves absolute equality when the frequency tends to infinity, as only then can G_n be truly neglected. Thus,

$$G_n = \frac{G_0}{j2\pi f C_0} \implies G_n \propto \frac{1}{f} \quad (29)$$

$$\lim_{f \rightarrow \infty} G_n = 0 \quad (30)$$

However, this argument only holds if we neglect that G_0 itself is a function of the frequency, i.e. $G_0(\omega)$, and is predicted to vary as ω^4 . Thus it is very hard to predict accurately the permittivity without taking into account that G_0 varies with the frequency. Additionally, the short circuit simplification was utilized, assuming that the short behaves as a zero impedance, resulting in infinite admittance. However, this simplification overlooks the complexities of real-world factors. In reality, even without considering superconductivity, it is impossible to achieve exactly zero impedance, and thus infinite admittance. Therefore, the most accurate equation for determining the complex permittivity of a material would be Equation 20. However, solving this equation is considerably more challenging as it requires first determining G_n by introducing a material with known permittivity and reflection coefficient. Despite its complexity, it can be solved using numerical analysis and solutions (Marsland & Evans, 1987).

In conclusion, this project successfully developed a radiating antenna model based on the methodology proposed by Marsland and Evans. Through a comparison with a conventional equivalent circuit approach, we determined the complex permittivities of methanol (CH_3OH) and sodium chloride (NaCl). Remarkably, the obtained complex permittivities closely matched theoretical predictions, particularly at higher frequencies, demonstrating the effectiveness of the proposed antenna model in simulating the behavior of a coaxial transmission line. However, discrepancies were observed, especially at lower frequencies, where experimental values deviated from theoretical predictions to a greater extent. Despite this, the model showed promising accuracy in capturing the complex behavior of the transmission line and provided valuable insights into the interaction between electromagnetic waves and materials.

REFERENCES

- Analysis, C S (n.d.) *FDTD vs. FEM vs. MOM: What are they and how are they different?* <https://resources.system-analysis.cadence.com/blog/msa2021-fdtd-vs-fem-vs-mom-what-are-they-and-how-are-they-different> Accessed on March 3, 2024.
- Brandy, M Symons, S & Stuchly, S (1981) Dielectric behavior of selected animal tissues in vitro at frequencies from 2 to 4 ghz. *IEEE Transactions on Biomedical Engineering*, (3) 305–307.
- Chen, W K (2004) *The electrical engineering handbook*. Elsevier.
- Deschamps, G (1962) Impedance of an antenna in a conducting medium. *IRE Transactions on Antennas and Propagation*, 10(5) 648–650.
- Kraszewski, A Stuchly, M A & Stuchly, S S (1983) Ana calibration method for measurements of dielectric properties. *IEEE Transactions on Instrumentation and Measurement*, 32(2) 385–387.
- La Gioia, A Porter, E Merunka, I Shahzad, A Salahuddin, S Jones, M & O'Halloran, M (2018) Open-ended coaxial probe technique for dielectric measurement of biological tissues: Challenges and common practices. *Diagnostics*, 8(2) <https://doi.org/10.3390/diagnostics8020040>
- Marcuvitz, N (1951) *Waveguide handbook*. Iet.
- Marsland, T & Evans, S (1987) Dielectric measurements with an open-ended coaxial probe. *IEE Proceedings H (Microwaves, Antennas and Propagation)*, 134(4) 341–349.
- Rautio, J C (2014) *The long road to Maxwell's equations*. <https://spectrum.ieee.org/the-long-road-to-maxwells-equations> Accessed on February 25, 2024.
- Šarolić, A & Matković, A (2022) Dielectric permittivity measurement using open-ended coaxial probe-modeling and simulation based on the simple capacitive-load model. *Sensors*, 22(16) 6024. <https://doi.org/10.3390/s22166024>
- Von Hippel, A & Labounsky, A (1995) *Dielectrics and waves*. Artech House. <https://books.google.com.mt/books?id=IfOLQQAACAAJ>

APPENDIX

1 CODE LISTING

```
33 # Defining the reflection coefficients
34 F = np.array(data["F"])/1e9
35 A_r = np.array(data["A_R"] + 1j * data["A_I"])
36 W_r = np.array(data["W_R"] + 1j * data["W_I"])
37 M_r = np.array(data["M_R"] + 1j * data["M_I"])
38 N_r = np.array(data["N_R"] + 1j * data["N_I"])
39 S_r = np.array(data["S_R"] + 1j * data["S_I"])
40
41 rho_m = N_r
42
43 # Delta_ij = rho_i - rho_j
44 Dm2 = rho_m - A_r
45 D13 = S_r - W_r
46 Dm1 = rho_m - S_r
47 D32 = W_r - A_r
48 Dm3 = rho_m - W_r
49 D21 = A_r - S_r
50 Dm1 = rho_m - S_r
51 D32 = W_r - A_r
52
53 # Experimental permittivity of NaCl
54 e_NaCl = -((Dm2*D13*e_W) / (Dm1*D32)) - ((Dm3*D21*e_A) / (Dm1*D32))
55 e_Nreal = e_NaCl.real
56 e_Nimag = -1*e_NaCl.imag
57 e_Nabs = abs(e_NaCl)
58
59
60 rho_m = M_r
61
62
63 Dm2 = rho_m - A_r
64 D13 = S_r - W_r
65 Dm1 = rho_m - S_r
66 D32 = W_r - A_r
67 Dm3 = rho_m - W_r
68 D21 = A_r - S_r
69 Dm1 = rho_m - S_r
70 D32 = W_r - A_r
71
72 # Experimental permittivity CH_3OH
73 e_methanol = -((Dm2*D13*e_W) / (Dm1*D32)) - ((Dm3*D21*e_A) / (Dm1*D32))
```

```
74 e_Mreal = e_methanol.real
75 e_Mimag = -1*e_methanol.imag
76 e_Mabs = abs(e_methanol)
77
78
79 # Determining the residuals for Each graph, its accuraries and plotting respectively
80 residuals1 = e_Nreal - e_NR
81 Accur = abs(((e_Nreal/e_NR)-1)*100)
82
83
84 fig, (ax1, ax2) = plt.subplots(2, 1, figsize=(11, 15), gridspec_kw={'height_ratios': [4,
     1] })
85
86
87 ax1.plot(F, e_NR, label=r'Theoretical Values', zorder=2)
88 ax1.scatter(F, e_NR, s=20, zorder=2)
89
90
91 ax1.errorbar(F[::3], e_Nreal[::3], yerr=Accur[::3], fmt='o', color='black', ecolor='grey',
    markersize=1, zorder=1)
92
93
94 ax1.plot(F, e_Nreal, label=r'Experimental Values', color = 'orange',zorder = 2)
95 ax1.scatter(F, e_Nreal, s=20, color='orange', zorder= 2)
96
97
98
99 ax1.minorticks_on()
100 ax1.grid(visible=True, which='major', linestyle='--')
101 ax1.grid(visible=True, which='minor', linestyle='---')
102 ax1.set_title(r'A Graph showing the real part of the complex permittivity of NaCl in Fm$^{-1}$ against frequency in Hz')
103 ax1.set_ylabel(r'$\varepsilon' \prime_{NaCl} / Fm^{-1}$')
104 ax1.legend()
105
106
107 ax2.plot(F, residuals1, color='black')
108 ax2.scatter(F, residuals1, color='black')
109 ax2.axhline(0, color='black', linewidth=0.5)
110 ax2.minorticks_on()
111 ax2.grid(visible=True, which='major', linestyle='--')
```

```
112 ax2.grid(visible=True, which='minor', linestyle='--')
113 ax2.set_xlabel(r'$f$ / $10^9$ Hz')
114 ax2.set_ylabel(r'Residuals / $\mathbf{Fm}^{-1}$')
115
116
117 plt.subplots_adjust(hspace=0)
118 plt.savefig('Graph1', dpi=1000)
119 plt.show()
120
121 residuals2 = e_Nimag - e_NI
122
123 Accur1 = abs(((e_Nimag/e_NI)-1)*100)
124
125
126 fig, (ax1, ax2) = plt.subplots(2, 1, figsize=(11, 15), gridspec_kw={'height_ratios': [4,
127
128     1] })
129
130 ax1.plot(F, e_NI, label=r'Theoretical Values', zorder = 1)
131 ax1.scatter(F, e_NI, s=20, zorder = 1)
132
133 ax1.errorbar(F[::3], e_Nimag[::3], yerr=Accur1[::3], fmt='o', color='black', ecolor='grey',
134     markersize=1, zorder=1)
135
136
137
138 ax1.minorticks_on()
139 ax1.grid(visible=True, which='major', linestyle='-')
140 ax1.grid(visible=True, which='minor', linestyle='--')
141 ax1.set_title(r'A Graph showing the imaginary part of the complex permittivity of NaCl in
142     $\mathbf{Fm}^{-1}$ against frequency in Hz')
143 ax1.set_ylabel(r'$\varepsilon' \prime \prime_{NaCl} / \mathbf{Fm}^{-1}$')
144 ax1.legend()
145
146
147
148 ax2.plot(F, residuals2, color='black')
149 ax2.scatter(F, residuals2, color='black')
```

```
150 ax2.axhline(0, color='black', linewidth=0.5)
151 ax2.minorticks_on()
152 ax2.grid(visible=True, which='major', linestyle='--')
153 ax2.grid(visible=True, which='minor', linestyle='---')
154 ax2.set_xlabel(r'$f / 10^9$ Hz')
155 ax2.set_ylabel(r'Residuals / $Fm^{-1}$')
156
157
158 plt.subplots_adjust(hspace=0)
159 plt.savefig('Graph2', dpi=1000)
160 plt.show()
161
162
163 residuals3 = e_Nabs - e_NA
164 Accur2 = abs(((e_Nabs/e_NA)-1)*100)
165
166
167 fig, (ax1, ax2) = plt.subplots(2, 1, figsize=(11, 15), gridspec_kw={'height_ratios': [4,
168
169
170 ax1.plot(F, e_NA, label=r'Theoretical Values', zorder=1)
171 ax1.scatter(F, e_NA, s=20, zorder=1)
172
173
174 ax1.errorbar(F[::3], e_Nabs[::3], yerr=Accur2[::3], fmt='o', color='black', ecolor='black',
175
176 ax1.plot(F, e_Nabs, label=r'Experimental Values', zorder=1)
177 ax1.scatter(F, e_Nabs, s=20, zorder=1)
178
179
180
181 ax1.minorticks_on()
182 ax1.grid(visible=True, which='major', linestyle='--')
183 ax1.grid(visible=True, which='minor', linestyle='---')
184 ax1.set_title(r'A Graph showing the absolute value of the complex permittivity of NaCl in
185
186 ax1.set_ylabel(r'$|\varepsilon_{\mathrm{NaCl}}| / Fm^{-1}$')
187 ax1.legend()
```

```
188
189
190 ax2.plot(F, residuals3, color='black')
191 ax2.scatter(F, residuals3, color='black')
192 ax2.axhline(0, color='black', linewidth=0.5)
193 ax2.minorticks_on()
194 ax2.grid(visible=True, which='major', linestyle='--')
195 ax2.grid(visible=True, which='minor', linestyle='---')
196 ax2.set_xlabel(r'$f$ / $10^9$ Hz')
197 ax2.set_ylabel(r'Residuals / Fm$^{-1}$')
198
199
200 plt.subplots_adjust(hspace=0)
201 plt.savefig('Graph3', dpi=1000)
202 plt.show()
203
204
205 residuals4 = e_Mreal - e_MR
206
207 Accur3 = abs(((e_Mreal/e_MR)-1)*100)
208
209 fig, (ax1, ax2) = plt.subplots(2, 1, figsize=(11, 15), gridspec_kw={'height_ratios': [4,
210
211
212 ax1.plot(F, e_MR, label=r'Theoretical Values', zorder =2)
213 ax1.scatter(F, e_MR, s=20, zorder =2)
214 ax1.errorbar(F[::3], e_Mreal[::3], yerr=Accur3[::3], fmt='o', color='black', ecolor='grey',
215 markersize=1, zorder=1)
216 ax1.plot(F, e_Mreal, label=r'Experimental Values', zorder =2)
217 ax1.scatter(F, e_Mreal, s=20, zorder =2)
218
219
220 ax1.minorticks_on()
221 ax1.grid(visible=True, which='major', linestyle='--')
222 ax1.grid(visible=True, which='minor', linestyle='---')
223 ax1.set_title(r'A Graph showing the real part of complex permittivity of Methanol in Fm$^{-1}$ against frequency in Hz')
224 ax1.set_ylabel(r'$\varepsilon'(\omega_{\text{CH}_3\text{OH}})$ / Fm$^{-1}$')
225 ax1.legend()
```

```
226
227
228 ax2.plot(F, residuals4, color='black')
229 ax2.scatter(F, residuals4, color='black')
230 ax2.axhline(0, color='black', linewidth=0.5)
231 ax2.minorticks_on()
232 ax2.grid(visible=True, which='major', linestyle='--')
233 ax2.grid(visible=True, which='minor', linestyle='---')
234 ax2.set_xlabel(r'$f$ / $10^9$ Hz')
235 ax2.set_ylabel(r'Residuals / $\Delta\epsilon_{\text{MI}}$')
236
237
238 plt.subplots_adjust(hspace=0)
239 plt.savefig('Graph4', dpi=1000)
240 plt.show()
241
242
243 fig, (ax1, ax2) = plt.subplots(2, 1, figsize=(11, 15), gridspec_kw={'height_ratios': [4,
244
245
246 residuals = e_Mimag - e_MI
247
248 Accur4 = abs(((e_Mimag/e_MI)-1)*100)
249
250 ax1.plot(F, e_MI, label=r'Theoretical Values', zorder=2)
251 ax1.scatter(F, e_MI, s=20, zorder=2)
252
253 ax1.errorbar(F[::3], e_Mimag[::3], yerr=Accur4[::3], fmt='o', color='black', ecolor='grey',
254
255 markersize=1, zorder=1)
256
257 ax1.plot(F, e_Mimag, label=r'Experimental Values', zorder=2)
258 ax1.scatter(F, e_Mimag, s=20, zorder=2)
259
260 ax1.minorticks_on()
261 ax1.grid(visible=True, which='major', linestyle='--')
262 ax1.grid(visible=True, which='minor', linestyle='---')
263 ax1.set_title(r'A Graph showing the imaginary part of complex permittivity of Methanol in
264
265 $\Delta\epsilon_{\text{MI}}$ against frequency in Hz')
266 ax1.set_ylabel(r'$\Delta\epsilon_{\text{MI}}$ / $\Delta\epsilon_{\text{MI}}$')
267 ax1.set_ylim(0, 23)
```

```
264 ax1.legend()
265
266
267 ax2.plot(F, residuals, color='black')
268 ax2.scatter(F, residuals, color='black')
269 ax2.axhline(0, color='black', linewidth=0.5)
270 ax2.minorticks_on()
271 ax2.grid(visible=True, which='major', linestyle='--')
272 ax2.grid(visible=True, which='minor', linestyle='---')
273 ax2.set_xlabel(r'$f$ / $10^9$ Hz')
274 ax2.set_ylabel(r'Residuals / Fm$^{-1}$')
275
276 plt.subplots_adjust(hspace=0)
277 plt.savefig('Graph5', dpi=1000)
278 plt.show()
279
280 Accur5 = abs(((e_Mabs/e_MA)-1)*100)
281
282
283 fig, (ax1, ax2) = plt.subplots(2, 1, figsize=(11, 15), gridspec_kw={'height_ratios': [4,
284 1] })
285
286
287 residuals6 = e_Mabs - e_MA
288
289 ax1.plot(F, e_MA, label=r'Theoretical Values', zorder = 2)
290 ax1.scatter(F, e_MA, s=20, zorder = 2)
291 ax1.errorbar(F[::3], e_Mabs[::3], yerr=Accur5[::3], fmt='o', color='black', ecolor='grey',
292 markersize=1, zorder=1)
293
294 ax1.plot(F, e_Mabs, label=r'Experimental Values', zorder = 2)
295 ax1.scatter(F, e_Mabs, s=20, zorder = 2)
296
297
298 ax1.minorticks_on()
299 ax1.grid(visible=True, which='major', linestyle='--')
300 ax1.grid(visible=True, which='minor', linestyle='---')
301 ax1.set_title(r'A Graph showing the absolute value of the complex permittivity of Methanol
in Fm$^{-1}$ against frequency in Hz')
```

```
302 ax1.set_ylabel(r'$|\varepsilon_{\mathrm{r}} - \varepsilon_{\mathrm{OH}}| / Fm^{-1}$')
303 ax1.legend()
304
305
306 ax2.plot(F, residuals6, color='black')
307 ax2.scatter(F, residuals6, color='black')
308 ax2.axhline(0, color='black', linewidth=0.5)
309 ax2.minorticks_on()
310 ax2.grid(visible=True, which='major', linestyle='--')
311 ax2.grid(visible=True, which='minor', linestyle='---')
312 ax2.set_xlabel(r'$f / 10^9$ Hz')
313 ax2.set_ylabel(r'Residuals / $Fm^{-1}$')
314
315 plt.subplots_adjust(hspace=0)
316 plt.savefig('Graph6', dpi=1000)
317 plt.show()
```

Listing 1. Showing the code for figure 3 - 8

2 APPENDIX B

In Listing 1, the code for Figures 3 through 8 was developed. Initially, the packages NumPy, Matplotlib, and Pandas were imported. The Excel sheet containing the reflective coefficient and the theoretical values of the complex permittivity for NaCl, methanol, and distilled water was imported. Each variable was defined, respectively, and stored. Calculations were then performed to find the real and imaginary permittivity of NaCl and methanol. Finally, graphs of permittivity against frequency were plotted (real and imaginary separately), along with the theoretical values.